APPLICATION OF HIERARCHICAL HIGHER-ORDER TANGENTIAL VECTOR FINITE ELEMENTS IN A HYBRID FEM/MOM METHOD

Hao Wang, ChunLei Guo, and Todd H. Hubing
Department of Electrical and Computer Engineering
University of Missouri-Rolla
Rolla, MO 65409

ABSTRACT

Hybrid FEM/MoM methods combine the finite element method (FEM) and the method of moments (MoM) to model inhomogeneous unbounded problems. These two methods are coupled by enforcing field continuity on the boundary that separates the FEM and MoM regions. Hierarchical higher-order tangential vector finite elements (TVFE's) are of practical interest because they can be easily combined with low-order elements to improve the accuracy of numerical solutions. This paper presents a hybrid FEM/MoM formulation applying a set of hierarchical TVFE's developed by Webb and Forghani. Higher-order FEM elements are coupled to MoM elements based on *Rao-Wilton-Glisson (RWG)* functions. The FEM matrix assembly procedure is described in sufficient detail to aid other investigators who wish to develop codes employing this technique. Three practical electromagnetic problems are presented that demonstrate the advantages of the higher-order elements.

I. INTRODUCTION

The hybrid finite-element-method and method-of-moments (FEM/MoM) can be used to analyze many kinds of electromagnetic problems effectively by applying FEM to model the fields in regions with geometric complexity and using MoM to model larger, simpler structures outside this region and to provide an accurate radiation boundary condition (RBC) to terminate the FEM mesh. Both the MoM and FEM are powerful methods, but each of these methods has its own advantages and disadvantages. MoM handles unbounded problems very effectively but is less efficient when complex inhomogeneities are present. Inhomogeneities are easily handled by the FEM, which requires less computer time and storage. However, the FEM is most suitable for bounded problems. Hence, hybrid FEM/MoM methods that combine MoM and FEM are advantageous for treating electromagnetic problems involving unbounded, complex structures.

Conventional hybrid FEM/MoM codes employ linear tangential vector finite elements (TVFE's). These elements are commonly referred to as Whitney elements defined by Nedelec [1]. Because the functions do not impose normal component continuity between tetrahedra, they do not produce the spurious modes that can be generated by using node-based elements [2]. However, these elements limit the accuracy of the finite element solution since they only support a constant tangential value along element edges and a linear field variation inside the element (CT/LN). Thus, when electric fields in a certain region vary quickly, the number of tetrahedra has to be relatively high to obtain reasonable accuracy. Higher-order elements that support non-linear field variations can be used to model rapidly varying fields using fewer elements. One set of higher-order basis functions for tetrahedra supports a linear tangential, quadratic normal (LT/QN) representation of the fields. Basis functions of the next higher order have a quadratic tangential, cubic normal (QT/CuN) representation for the fields. A set of TVFE's is referred to as interpolatory if values within the element can be interpolated from node or edge values. It is referred to as hierarchical if the lower-order basis functions are a subset of the higher order basis functions. Webb and Forghani [3], Savage and Peterson [4], Graglia *et al*. [5], and Andersen and Volakis [6] have employed LT/QN basis functions. The TVFE's presented in [4] and [5] are interpolatory while those presented in [3] and [6] form a hierarchical set with the Whitney TVFE. Hierarchical sets of TVFE's allow for selective field expansion using different order elements in different regions of the computational domain. Hence, for the regions where the fields vary slowly, the lowest order TVFE's can be employed, while for the regions where the fields vary rapidly, higher-order TVFE's can be employed. This can save memory and CPU time without compromising computational accuracy. Andersen developed and applied mixed-order hierarchical TVFE's in [7].

For MoM techniques based on EFIE formulations, Nedelec [1] presented a general family of divergence-conforming functions whose lowest-order member was a set of CN/LT basis functions, known as *Rao-Wilton-Glisson (RWG)* or *triangular rooftop* functions. These functions are widely used for representing surface currents in EFIE formulations.

In a hybrid FEM/MoM technique, hierarchical sets of TVFE's are readily coupled to linear MoM boundary elements because the coefficients corresponding to any higher-order terms on the boundary can be set to zero to enforce the continuity of the tangential fields.

The coefficient matrices generated by FEM/MoM codes may have large condition numbers. When LT/QN basis functions are used in the FEM, the condition numbers of the hybrid matrix generally become much larger. Savage [8] showed that interpolatory vector basis functions are generally better conditioned than hierarchical vector basis functions. However, only the condition numbers of individual element matrices were studied in [8]. Andersen [9] examined the inter-relationships between the condition numbers of element and global matrices based on various interpolatory and hierarchical TVFE's using a cavity resonator example. However because they were solving for the eigenvalues of a cavity resonator, the condition numbers of the global FEM matrices were not considered.

In this paper, the hybrid FEM/MoM formulation using the LT/QN TVFE's described by Webb and Forghani in [3] is developed and applied to different electromagnetic problems. Section II presents the hybrid FEM/MoM formulation. Section III presents the FEM matrix assembly procedure for LT/QN TVFE's. Section IV presents a set of numerical results that demonstrates the improved performance of the higher-order TVFE in the context of the 3-D hybrid FEM/MoM.

II. FORMULATION

In the hybrid FEM/MoM, an electromagnetic problem is divided into an interior equivalent part and an exterior equivalent part. The interior part is modeled using the FEM and the exterior part is modeled using a surface integral equation method-of-moments technique (MoM). The two equivalent parts are coupled by enforcing the continuity of tangential fields on the FEM and MoM boundary [10].

2.1 The Finite Element Method Using Higher - Order TVFE's

FEM can be used to analyze the interior equivalent part by solving the weak form of the vector wave equation as follows [7]:

$$\int_V \left[\left(\frac{\nabla \times \mathbf{E}(\mathbf{r})}{j\,\omega\,\mu_0\mu_r} \right) \bullet (\nabla \times \mathbf{w}(\mathbf{r})) + j\,\omega\,\varepsilon_0\varepsilon_r \mathbf{E}(\mathbf{r}) \bullet \mathbf{w}(\mathbf{r}) \right] dV$$

$$= \int_S (\hat{n} \times \mathbf{H}(\mathbf{r})) \bullet \mathbf{w}(\mathbf{r})\, dS - \int_V \mathbf{J}^{\mathrm{int}}(\mathbf{r}) \bullet \mathbf{w}(\mathbf{r})\, dV \qquad (1)$$

where S is the surface enclosing volume V, $\mathbf{w(r)}$ is the weighting function, and $\mathbf{J}^{\mathrm{int}}$ is an impressed source. Equation (1) shows that efficient finite-element analysis of electromagnetic fields in 3-D regions requires computation of two element matrices. These two matrices are

$$E_{ij} = \int_V \nabla \times \mathbf{w}_i \bullet \nabla \times \mathbf{w}_j\, dV \qquad (2)$$

$$F_{ij} = \int_V \mathbf{w}_i \bullet \mathbf{w}_j\, dV \qquad (3)$$

where $\mathbf{w}_i$ represents the i*th* vector basis function and V indicates integration over one tetrahedron. The six edges and four faces of a tetrahedron are numbered as indicated in Table 1 and Figure 1 [4].

Table 1. Node and edge numbering scheme of a tetrahedron

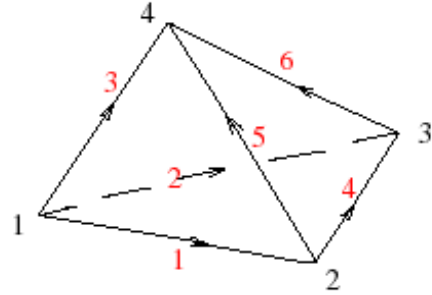| Edge#	Node 1	Node 2	
1	1	2	
2	1	3	
3	1	4	
4	2	3	
5	2	4	
6	3	4	
Face#	Node 1	Node 2	Node 3
1	1	2	3
2	1	2	4
3	1	3	4
4	2	3	4

Figure 1. Edge and face definition of a tetrahedron.

The linear-tangential, quadratic-normal (LT/QN) basis functions developed by Webb exist in two forms. One is edge-based functions, which are associated with tetrahedron edges. The other is face-based functions, which are associated with tetrahedron faces. The two edge-based LT/QN basis functions associated with edge *i* are,

$$\mathbf{w}_k^{\mathbf{e1}} = l_k(L_{k1}\nabla L_{k2} - L_{k2}\nabla L_{k1}) \quad k = 1,\cdots,6 \qquad (4)$$

$$\mathbf{w}_k^{\mathbf{e2}} = l_k(L_{k1}\nabla L_{k2} + L_{k2}\nabla L_{k1}) \quad k = 1,\cdots,6 \qquad (5)$$

where "e1" represents the first type of edge basis function, and "e2" represents the second type of edge

basis function. L_i is the area coordinate associated with the node i. It is unity at node i and decays in a linear fashion to zero at the other three nodes of the cell. l_i is the length of edge i.

Figure 2 shows vector plots of the edge-based functions in a face of a tetrahedron. The two face-based elements associated with face i are,

$$\mathbf{w}_i^{f1} = L_{i1}L_{i2}\nabla L_{i3} - L_{i1}L_{i3}\nabla L_{i2} \quad i = 1,\cdots 4 \qquad (6)$$

$$\mathbf{w}_i^{f2} = L_{i1}L_{i2}\nabla L_{i3} - L_{i2}L_{i3}\nabla L_{i1} \quad i = 1,\cdots 4 \qquad (7)$$

where "$f1$" represents the first type of face basis function, and "$f2$" represents the second type of face basis function. Figure 3 shows vector plots of the face-based functions on a face of a tetrahedron. It shows that the field distributions in $f1$ elements and $f2$ elements are similar but they rotate in different directions.
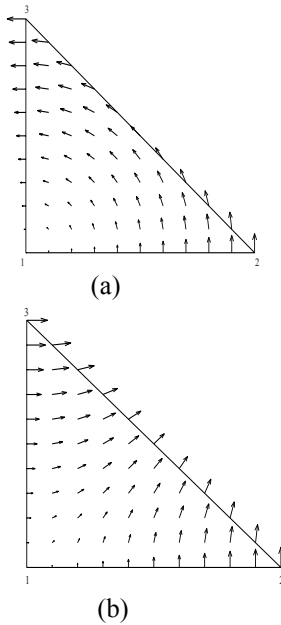

(a)

(b)

Figure 2. Plot of the edge based basis functions. (a) $\mathbf{w}_i^{e1}$, (b) $\mathbf{w}_i^{e2}$.

Using these basis functions, the electric field **E** in the interior region can be expanded as the sum of four terms,

$$\mathbf{E(r)} = \sum_{k=1}^{N_v}(E_k^{e1}\mathbf{w}_k^{e1} + E_k^{e2}\mathbf{w}_k^{e2} + E_k^{f1}\mathbf{w}_k^{f1} + E_k^{f2}\mathbf{w}_k^{f2})\cdot \quad (8)$$

The basis function $\mathbf{w}_k$ has the following properties:

$$\mathbf{e}_k \bullet \mathbf{w}_k^{e1} = l_k\frac{L_{k1}+L_{k2}}{l_k} = L_{k1}+L_{k2} = 1 \qquad (9)$$

$$\mathbf{e}_k \bullet \mathbf{w}_k^{e2} = l_k\frac{L_{k1}-L_{k2}}{l_k} = L_{k1}-L_{k2} \qquad (10)$$

where $\mathbf{e}_k$ is a unit edge vector corresponding to the kth edge. Hence, the terms associated with "$e1$" elements can be viewed as the *main* terms that describe fields along tetrahedron edges roughly, while the terms associated with "$e2$" elements can be viewed as *adjustment* terms that describe the field's linear variation along tetrahedron edges.
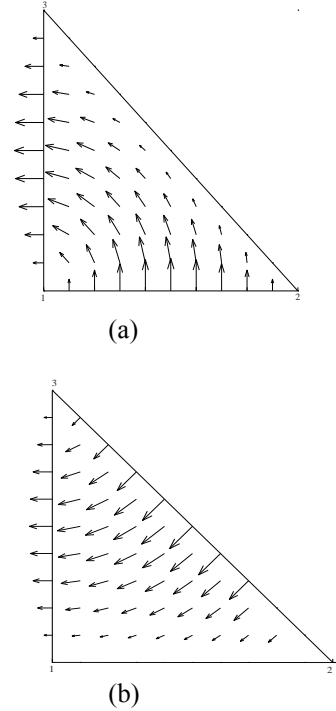

(a)

(b)

Figure 3. Plot of the face based basis functions, (a) $\mathbf{w}_i^{f1}$, (b) $\mathbf{w}_i^{f2}$.

Since CT/LN functions have one unknown per edge, they generate 6×6 local matrices. LT/QN functions have two unknowns per edge and two unknowns per face so they generate 20×20 local matrices. Applying the LT/QN basis functions to (1), a global FEM matrix can be constructed as follows,

$$\begin{bmatrix} A_{ii}^{e1e1} & A_{id}^{e1e1} & A_{ii}^{e1e2} & A_{ii}^{e1f} \\ A_{di}^{e1e1} & A_{dd}^{e1e1} & A_{di}^{e1e2} & A_{di}^{e1f} \\ A_{ii}^{e2e1} & A_{id}^{e2e1} & A_{ii}^{e2e2} & A_{ii}^{e2f} \\ A_{ii}^{fe1} & A_{id}^{fe1} & A_{ii}^{fe2} & A_{ii}^{ff} \end{bmatrix}\begin{bmatrix} E_i^{e1} \\ E_d^{e1} \\ E_i^{e2} \\ E_i^{f} \end{bmatrix} =$$

$$\begin{bmatrix} 0 & 0 \\ 0 & B_{dS} \end{bmatrix}\begin{bmatrix} 0 \\ J_S \end{bmatrix} + \begin{bmatrix} g^{int} \end{bmatrix}. \qquad (11)$$

The unknown coefficients $[E_n]$ are partitioned into four types according to their corresponding basis functions and edge functions. The four categories are interior edges of "$e1$" type, which are denoted by the subscript i, dielectric boundary edges of type "$e1$", which are denoted by the subscript d, interior edges of type "$e2$", and interior faces of type "f", which are

also denoted by the subscript i. The type "$f1$" and type "$f2$" basis functions have been combined into one common "f" type because they are essentially the same when they share the same face and rotate along the same edge. E_k^{e2}, E_k^{f1} and E_k^{f2} are set equal to zero on the MoM boundary to enforce the continuity of the tangential electric fields. Using this approach, the MoM part (employing linear basis functions) does not have to be modified to work with FEM elements of different order. $[J_s]$ is a set of unknown complex scalar coefficients for the surface electric current densities on the FEM and MoM boundary S. $[g^{int}]$ is the source term, representing sources located within the FEM region. The elements of $[A]$, $[B_{dS}]$, and $[g^{int}]$ are given by,

$$A_{mn} = \int_V [\frac{(\nabla \times \mathbf{w_n(r)}) \bullet (\nabla \times \mathbf{w_m(r)})}{j\omega\mu_0\mu_r}$$
$$+ j\omega\varepsilon_0\varepsilon_r \mathbf{w_n(r)} \bullet \mathbf{w_m(r)}]dV \qquad (12)$$

$$B_{mn} = \int_{S_d} \mathbf{f_n(r)} \bullet \mathbf{w_m(r)}dS \qquad (13)$$

$$g_m^{int} = -\int_V \left[\mathbf{J}^{int} + \frac{1}{j\omega\mu_0\mu_r}\left(\nabla \times \mathbf{M}^{int} \right) \right] \bullet \mathbf{w_m(r)}\, dV . \qquad (14)$$

2.2 The MoM Using EFIE

The exterior equivalent part can be analyzed using the EFIE [8].

$$\frac{\mathbf{E(r)}}{2} = \mathbf{E}^{inc}(\mathbf{r}) + \int_S [-M(\mathbf{r'}) \times \nabla' G_0(\mathbf{r},\mathbf{r'})$$
$$- j\,k_0\,\eta_0 \mathbf{J(r')} \mathbf{G_0(r,r')} + j\frac{\eta_0}{k_0}\nabla' \bullet \mathbf{J(r')}\nabla' \mathbf{G_0(r,r')}]dS \qquad (15)$$

The equivalent surface electric current $\mathbf{J(r)}$ and magnetic current $\mathbf{M(r)}$ in (15) can be discretized using the *Rao-Wilton-Glisson* basis function $\mathbf{f(r)}$ [9].

$$\mathbf{J(r)} = \sum_{n=1}^{N_S} (J_s)_n \mathbf{f_n(r)} \qquad (16)$$

$$\mathbf{M(r)} = \sum_{n=1}^{N_d} (E_d^{e1})_n \mathbf{f_n(r)} \qquad (17)$$

where N_S is the total number of edges on the FEM and MoM boundary S, and N_d is the total number of edges on the dielectric boundary S_d. $\mathbf{E(r)}$ in Equation (15) can be expanded using the tetrahedral CT/LN basis function $\mathbf{w}^{e1}\mathbf{(r)}$ as follows,

$$\mathbf{E(r)} = \sum_{n=1}^{N_d} (E_d^{e1})_n \mathbf{w_n^{e1}(r)} \qquad (18)$$

On the surface S, the triangular basis function $\mathbf{f(r)}$ and the CT/LN basis function $\mathbf{w}^{e1}\mathbf{(r)}$ are related by,

$$\mathbf{w^{e1}(r)} = \hat{n} \times \mathbf{f(r)} . \qquad (19)$$

After multiplying by weighting functions $\mathbf{f_n(r)}$, n=1, ... N, the EFIE in Equation (15) can be discretized as follows,

$$[C][J_s] = [D][E_d^{e1}] - [F^i]. \qquad (20)$$

2.3 The Hybridization of FEM and MoM

Equations (11) and (20) form a coupled and determined system. Three different formulations, *the combined formulation*, *the inward-looking formulation and the outward-looking formulation*, can be used to solve the coupled system [11], [14]. The outward-looking formulation was used for the examples in this paper. From (20),

$$J_s = C^{-1}D\, E_d^{e1} - C^{-1}F^i . \qquad (21)$$

Substituting Equation (21) into Equation (11) yields a determined matrix equation,

$$\begin{bmatrix} A_{ii}^{e1e1} & A_{id}^{e1e1} & A_{ii}^{e1e2} & A_{ii}^{e1f} \\ A_{di}^{e1e1} & A_{dd}^{e1e1} - B_{dS}C^{-1}D & A_{di}^{e1e2} & A_{di}^{e1f} \\ A_{ii}^{e2e1} & A_{id}^{e2e1} & A_{ii}^{e2e2} & A_{ii}^{e2f} \\ A_{ii}^{fe1} & A_{id}^{fe1} & A_{ii}^{fe2} & A_{ii}^{ff} \end{bmatrix} \begin{bmatrix} E_i^{e1} \\ E_d^{e1} \\ E_i^{e2} \\ E_i^{f} \end{bmatrix} =$$

$$\begin{bmatrix} g_{int}^{e1} \\ g_{int}^{e2} \\ g_{int}^{f} \end{bmatrix} + [B_{dS}C^{-1}F^i] \qquad (22)$$

Equation (22) can be solved using iterative solvers. The preconditioning technique reported in [14] can be used to improve the convergence rate and accuracy of the iterative solvers.

III. ASSEMBLY

The aim of the assembly procedure in FEM is to construct the global matrix (11) by summing the element matrix terms for each tetrahedron in the mesh while guaranteeing continuity of the tangential electric field on the boundary between any two tetrahedra. For CT/LN basis functions, the assembly procedure is relatively straight-forward. However, for LT/QN basis functions, more details have to be considered in order to get the correct global matrix. This section describes the assembly procedure for LT/QN TVFE's.

For "$e1$" elements, Equation (4) and Figure 2(a) indicate that the complex scalar E_k^{e1} is the projection of the electric field onto the kth edge. When the local edge vector (as defined in Table 1) is reversed, Equation (4) will be reversed at the same time. Therefore, to ensure the continuity of the tangential

electric field across all edges, a unique global edge direction must be defined (e.g. always pointing from the smaller node number to the larger node number). Equation (4) must be multiplied by (-1) if the local edge vector does not have the same direction as the global edge direction.

For "*e2*" elements, the continuity of the tangential electric field across all edges must also be satisfied. From Figure 2 (b) and Equation (5), it is clear that when the local edge vector is reversed, there is no change in Equation (5). Therefore Equation (5) should not be multiplied by (-1) even when the local edge vector does not have the same direction as the global edge direction. When a FEM edge is on the boundary between FEM and MoM, E_k^{e2} associated with this edge is set to zero.

For "*f1*" and "*f2*" elements, the continuity of the tangential field needs to be enforced across all faces. From Figure 3, two local E_k^{f} can be regarded as a common global unknown only if they share the same face and rotate along the same edge. When the local edge vector, as defined in Table 1, is reversed, Equation (6) and Equation (7) will be reversed at the same time. Therefore, Equation (6) and Equation (7) should be multiplied by (-1) if the local edge vector does not have the same direction as the global edge direction.

As illustrated in Figure 4, there are generally four kinds of faces. In (a), the three edges of the face are all within the FEM volume. In (b), one or two edges of the face are on the FEM/MoM boundary. In (c), the three edges of the face are all on the FEM/MoM boundary while the area of the face is located in the FEM volume. In (d), the three edges and the area of the face are all on the FEM and MoM boundary. Normally, at the interface between higher-order FEM elements and CN/LT MoM elements, the higher-order terms, E_k^{f}, are set to zero. However, for the faces of type (a), (b) and (c), the complex scalar E_k^{f} rotating along the edge that is located on the FEM/MoM boundary, represents fields within the FEM volume and cannot be set to zero. Allowing these terms to have a non-zero value will not affect the coupling between FEM and MoM, since their projection on the boundary is equal to zero. For the faces of type (d), complex scalars E_k^{f1} and E_k^{f2} corresponding to this type must be set to zero.

IV. NUMERICAL RESULTS

This section describes three examples illustrating the performance of the hybrid FEM/MoM with CT/LN and LT/QN FEM basis functions. All matrices were solved using a biconjugate gradient stabilized solver [11]. A 750-MHz Pentium III computer was used to perform the computation.
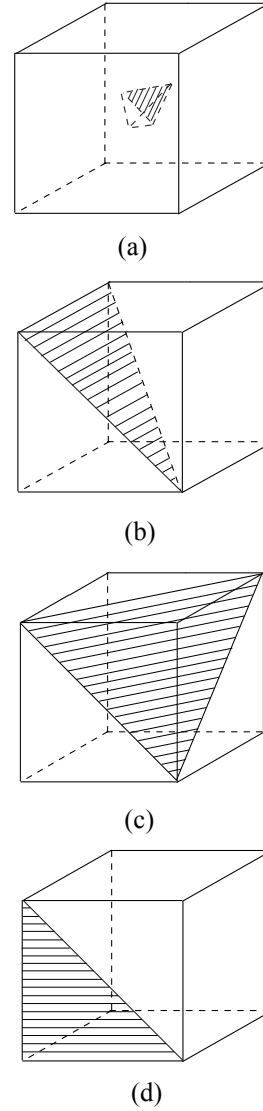

(a)

(b)

(c)

(d)

Figure 4. Faces in a tetrahedron.

4.1 The Scattered Field from a Sphere

This example models the scattering of an electromagnetic plane wave by a dielectric sphere. As shown in Figure 5, the radius of the sphere is 0.09 m and the relative permittivity is 4.5. The incident wave propagates in the $+\hat{z}$ direction. The wave has amplitude E_0 and is polarized in the $\hat{x}$ direction,

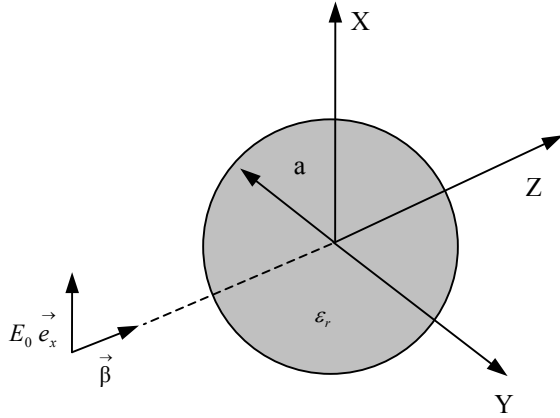$$\mathbf{E}(x,y,z,t) = E_0\mathbf{e}_x e^{j(wt-\beta z)}. \qquad (23)$$

Figure 5. Scattered field from a dielectric sphere.

Figure 6. Bistatic RCS of the dielectric sphere at 583 MHz.

A commercial software package was used to discretize the FEM volume with different densities to demonstrate the advantages of the proposed higher-order TVFE's. The MoM boundary was chosen to coincide with the physical boundary of the dielectric sphere. The number of MoM basis functions was fixed during the whole process. For validation, results using the Mie series [15] were compared to the FEM/MoM results. In Figure 6, we compare results for the three-dimensional bistatic scattering cross section at a frequency of 583 MHz. The Mie series result is denoted "Mie." For a mesh with a small number of tetrahedra, the result using the CT/LN TVFE is denoted "CT/LN TVFE coarse," and the result using the LT/QN TVFE is denoted "LT/QN TVFE coarse." For a mesh with a larger number of tetrahedra, the result using the CT/LN TVFE is denoted "CT/LN TVFE dense."

In Figure 6, the "CT/LN TVFE coarse" result is seen to compare fairly well with the exact Mie series result when the observation angle is between 100 degrees and 180 degrees. When the observation angle is below 100 degrees, a 1-dB discrepancy can be seen because the mesh is relatively coarse. For the denser mesh, the "CT/LN TVFE dense" result shows a significant improvement. By keeping the original coarse mesh and applying the LT/QN basis functions, the "LT/QN TVFE coarse" result agrees with the exact result very well. Even compared with the "CT/LN TVFE dense" result, the "LT/QN TVFE result" is closer to the exact result. Table 2 presents relevant parameters for the three results. Improved accuracy is obtained with less computer resources using LT/QN FEM basis functions.
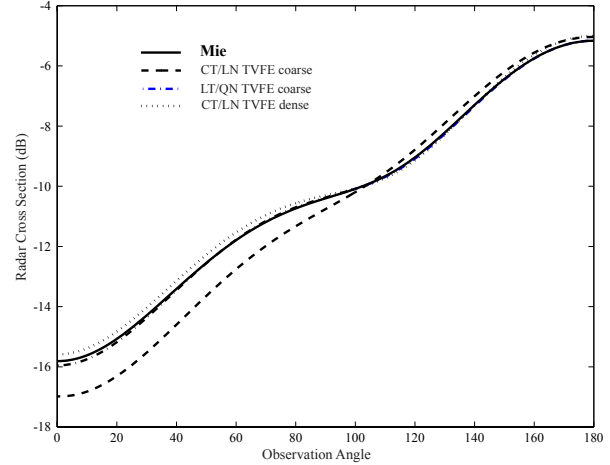
Table 2. Comparison between the results in Fig. 6

FEM Part	FEM Unkno-wns	MoM Unkno-wns	Average Edge Length (mm)	FEM Matrix Non - zeros	Solver Time (sec)
CT/LN Coarse	405	346	9.1	2379	28
CT/LN Dense	3266	346	4.3	18336	275
LT/QN Coarse	2430	346	9.1	51052	213

4.2 Input Impedance of a Power Bus Structure

This example models a printed circuit board (PCB) power bus structure. As shown in Figure 7, the board dimensions are 7.6 cm × 5.1 cm × 1.1 mm. The top and bottom planes are perfect electric conductors (PECs). The dielectric between the PEC layers has a relative permittivity of 3.81(1-j0.01). The MoM boundary is chosen to coincide with the physical boundary of the board. A source is identified at the location shown in Figure 7.
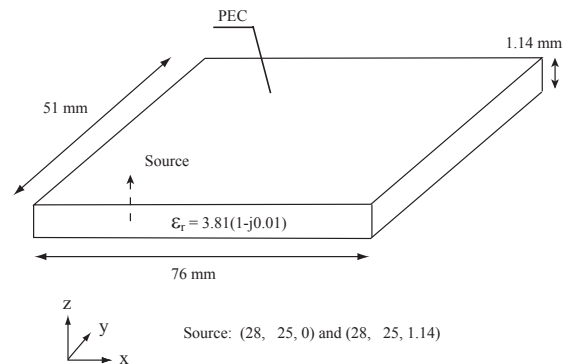

Figure 7. A PCB power bus structure.

Unlike the previous example, the fields in this configuration are relatively uniform. The electric field in the FEM region is vertically oriented and constant in the vertical direction. It is not obvious that a higher-order FEM element would benefit the analysis of this configuration.

The FEM uses a current filament on tetrahedron edges to model sources located within the FEM region [16]. A current source along the z-axis can be expressed as,

$$\mathbf{J}^{int} = I\delta(x - x_f)\delta(y - y_f)\hat{\mathbf{z}} \tag{24}$$

where (x_f, y_f) specifies its position, I denotes the electric current magnitude, and $\delta(x)$ is the Dirac delta function. The contribution to vector $[g^{int}]$ in Equation (24) is simply,

$$\mathbf{g}^{int} = I\iiint \hat{z}\bullet\{\mathbf{w}\}\delta(x - x_f)\delta(y - y_f)\,dxdydz \cdot \tag{25}$$

For an $e1$ basis function,

$$\mathbf{g}^{e1}_{int} = I\int_0^l l_1^e \frac{L_1^e + L_2^e}{l_1^e}\,dz = I\int_0^l dz = Il \cdot \tag{26}$$

For an $e2$ basis function,

$$\mathbf{g}^{e2}_{int} = I\int_0^l l_1^e \frac{L_1^e - L_2^e}{l_1^e}\,dz = 0 \cdot \tag{27}$$

For $f1$ and $f2$ basis functions

$$\mathbf{g}^{f}_{int} = 0 \tag{28}$$

since the tangential components of these functions along element edges are zero.

The power bus structure can also be modeled analytically as a cavity with two PEC and four perfect magnetic conductor (PMC) walls. The analytical resonance frequencies are given as follows (for $\mu_r = 1.0$) [17],

$$f_{m,n} = \frac{c}{2\pi\sqrt{\varepsilon_r}}\sqrt{\left(\frac{m\pi}{a}\right)^2 + \left(\frac{n\pi}{b}\right)^2} \quad m,n = 0,1,2,... \tag{29}$$

where a and b are the length and width of the cavity, respectively; m and n are the mode indices; c is the speed of light in free space; and ε_r is the relative permittivity of the material in the cavity. For this power bus structure, only TM_z modes are excited. From Equation (29), the $TM_z(1,0)$ mode's resonance frequency is 1011.1 MHz and the $TM_z(2,0)$ mode's resonance frequency is 2022.3 MHz.
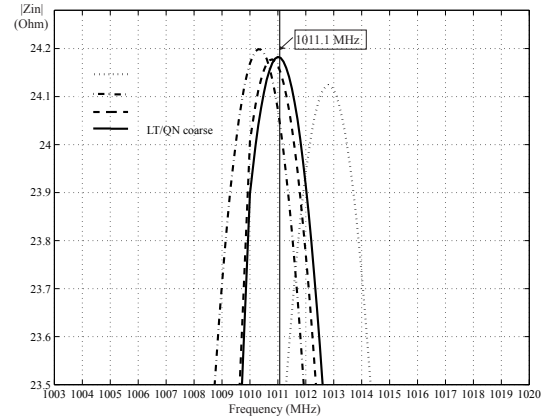
(a) $TM_z(1,0)$ mode
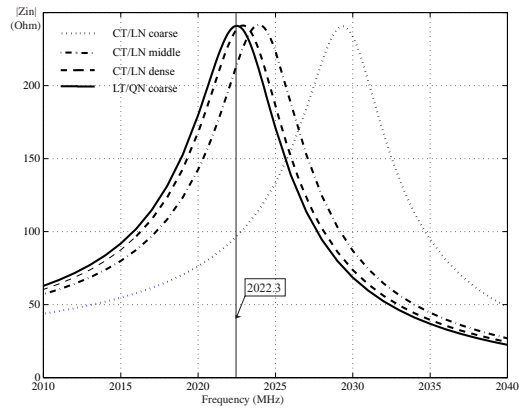
(b) $TM_z(2,0)$

Figure 8. Input impedance of the power bus structure.

In Figure 8, the computed input impedances of the power bus structure near these two resonance frequencies are compared. For a mesh with a number of tetrahedra between that of coarse mesh and dense mesh, the result using the CT/LN TVFE is denoted "CT/LN middle." The "LT/QN coarse" and "CT/LN coarse" examples employ the same mesh. It can be seen from Figure 8 that of the four cases, the "LT/QN coarse" results most accurately predict the resonance frequencies. Table 3 presents relevant parameters for the four cases. Once again the LT/QN coarse mesh yields more accurate results with fewer computer resources than a dense CT/LN mesh.

Table 3. Comparison between different formulations

Formulations	Unknowns	FEM non-zero	Solver time (sec)
CT/LN Coarse	467	4097	0.89
CT/LN Middle	1162	9940	1.54
CT/LN Dense	5041	42039	14.3
LT/QN Coarse	4124	87970	6.8

In [9], the inter-relationships between the condition numbers of individual elements as well as global matrices based on various interpolatory and hierarchical TVFE's were studied using a cavity resonator example. It was found that the LT/QN TVFE by Andersen and Volakis [7] resulted in better conditioned FEM matrices than the TVFE by Webb and Forghani. Since resonant structures like this power bus can be particularly susceptible to numerical error, this structure was also analyzed using higher-order elements based on the LT/QN elements in [7]. Figure 9 compares the condition numbers of the global FEM matrices generated by this example based on Andersen's and Webb's LT/QN basis functions. The term 'norm' denotes the normalized basis functions described in Appendix A. Up to 3 GHz, the LT/QN TVFE in [7] yields slightly better conditioned matrices than the TVFE in [5]. Normalized vector basis functions yield much smaller condition numbers than unnormalized vector basis functions.
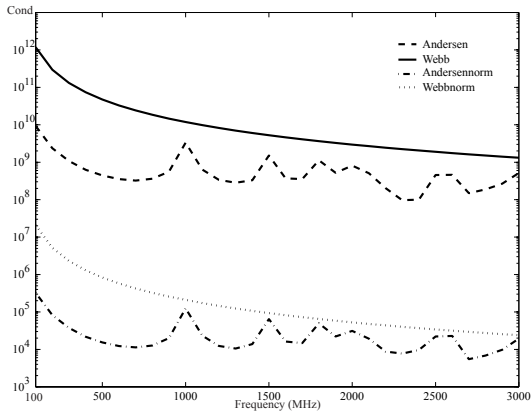

Figure 9. Condition numbers of the global FEM matrix based on different LT/QN basis functions.

4.3 Input Impedance of a Microstrip Structure

Numerical models of printed circuit board (PCB) geometries often include at least one microstrip structure (i.e. a trace over a plane). When these structures are modeled using a finite element technique with CT/LN basis elements, it is not uncommon to model the space between the trace and the plane with a single layer of elements. This approach generally yields good results when the trace is wide (e.g. the power bus structure) or when far-field results are calculated. However, for narrow traces or when calculating near-field properties (e.g. input impedance or crosstalk), a single layer of elements may not be adequate [16].
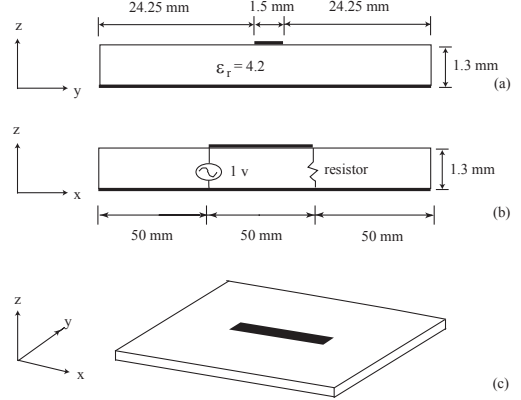

Figure 10. The geometry of a microstrip structure.

Figure 10 shows the geometry of a PCB with a thin trace. The trace width is only slightly greater than the trace height. The board is made of a dielectric with ε_r =4.2. The trace is excited by a current source at one end, and is terminated by a 47-ohm resistor at the other end. The MoM boundary is chosen to coincide with the physical boundary of the board.

The FEM code models load impedances Z_L as dielectric posts on tetrahedron edges [17]. Those posts have a finite conductivity given by

$$\sigma = \frac{l}{Z_L S} \tag{30}$$

where l is its length, and S is the cross sectional area. If the load is treated as a lumped element, its contribution to the finite element matrix is,

$$\left[A^{e1}\right] = \frac{l}{Z_L S} \iiint \left\{\mathbf{w}^{e1}\right\} \bullet \left\{\mathbf{w}^{e1}\right\}^T \delta(x - x_L)(y - y_L) dx dy dz = \frac{l^2}{Z_L} \tag{31}$$

for the *e1* basis function, and,

$$\begin{aligned}\left[A^{e2}\right] &= \frac{l}{Z_L S} \iiint \left\{\mathbf{w}^{e2}\right\} \bullet \left\{\mathbf{w}^{e2}\right\}^T \delta(x - x_L)(y - y_L) dx dy dz \\ &= \frac{l}{Z_L} \int_0^l (L_1 - L_2)^2 dz \\ &= \frac{l^2}{3Z_L}\end{aligned} \tag{32}$$

for the *e2* basis function, and,

$$\left[A^{f}\right] = 0 \tag{33}$$

for the *f1* and *f2* basis functions. The electric field lines around the trace are illustrated in Figure 11 [18]. Since the electric field around the trace varies

dramatically, the coarse mesh used to divide the FEM volume in the previous power bus example does not work here. Figure 11 also shows two meshes for a microstrip geometry. The coarse mesh is one element tall and the fine mesh is two elements tall.

Figure 12 shows the measured and calculated results for a 47-ohm termination up to 1 GHz. Note that the coarse mesh yields a poor result with CT/LN elements while the dense mesh results are close to the measured results. The LT/QN result with the coarse mesh also yields an accurate result.

(a)   Electric and magnetic field lines

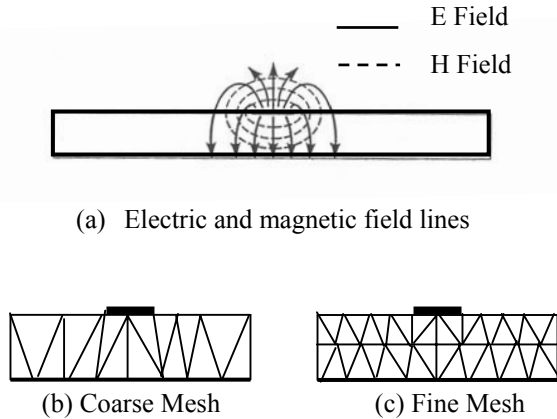(b) Coarse Mesh   (c) Fine Mesh

Figure 11. Cross-sectional view of the electric field and FEM meshes used to analyze the microstrip structure.
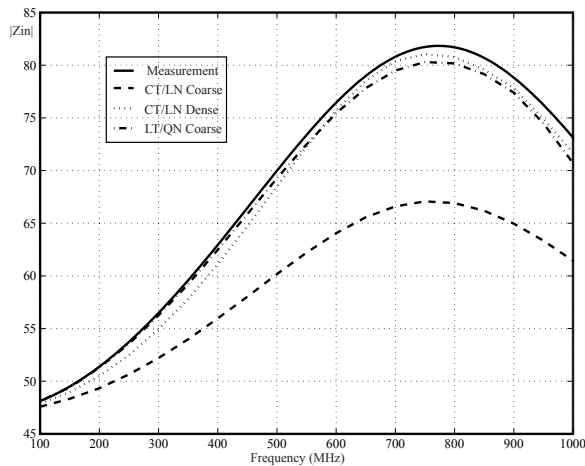

Figure 12. Input impedance of microstrip structure

VI. CONCLUSIONS

This paper presents a hybrid FEM/MoM formulation using higher-order (LT/QN) tangential vector finite elements. There are several kinds of LT/QN TVFE's. The basis functions developed by Webb and Forghani are applied here since they result in simpler

derivations compared to other hierarchical higher-order basis functions. The properties of the LT/QN basis functions are discussed and compared to traditional CT/LN basis functions. Three examples demonstrate that higher-order basis functions are capable of providing more accurate results with a coarser tetrahedral mesh and less computational resources. The condition numbers of the global FEM matrices derived from a power bus structure on the basis of various hierarchical LT/QN basis functions are compared. It is confirmed that the TVFE by Andersen results in somewhat better conditioned matrices than the TVFE by Webb and Forghani. Also, normalized vector basis functions are observed to result in much smaller condition numbers than unnormalized vector basis functions.

REFERENCES

[1]   J. C. Nedelec, "Mixed finite elements in R3," *Num. Math.*, vol. 35, pp. 315-341, 1980.

[2]   J. L. Volakis, A. Chatterjee, and L. C. Kempel, *Finite element method for electromagnetics*. New York: IEEE Press, 1998, ch. 2.

[3]   J. P. Webb and B. Forghani, "Hierarchical scalar and vector tetrahedra," *Digest of the Fifth Biennial IEEE Conference on Electromagnetic Field Computation*, Aug., 1992.

[4]   J. S. Savage and A. F. Peterson, "Higher-order vector finite elements for tetrahedral cells," *IEEE Trans. Microwave Theory Tech.*, vol. 44, pp. 874-879, June 1996.

[5]   R. Graglia, D. R. Wilton, and A. F. Petersen. "High order interpolatory vector bases for computational electromagnetics," *IEEE Transactions on Antennas and Propagation*, vol. AP-45, pp. 329-342, March 1997.

[6]   L. S. Andersen and J. L. Volakis, "Hierarchical tangential vector finite elements for tetrahedral," *IEEE Microwave and Guided Wave Letters*, vol. 8, pp. 127-129, no. 3, March 1998.

[7]   L. S. Andersen and J. L. Volakis, "Development and application of a novel class of hierarchical tangential vector finite elements for electromagnetics," *IEEE Transactions on Antenna and Propagation*, vol. AP-47, pp. 112-120, January 1999.

[8]   J. S. Savage. "Comparing high order vector basis functions," *Proc. Of the 14th Annual Review of Progress in Applied Computational Electromagnetics*, Monterey, CA, USA, pp. 524-529, March 1999.

[9]   L. S. Andersen and J. L. Volakis, "Condition numbers for various FEM matrices," *Journal of Electromagnetic Waves and Applications*, vol. 13, pp. 1661-1677. December 1999.

[10]   Y. Ji and T. H. Hubing, "EMAP5: A 3D hybrid FEM/MoM code," *Appl. Computat. Electromagn. Soc. (ACES) J.*, vol. 15, pp. 1-12, March 2000.

[11]   A. F. Petersen, S. L. Ray, and R. Mittra, *Computational Methods for Electromagnetics*, New York: IEEE Press and Oxford University Press, 1997.

[12]   J. J. H. Wang, *Generalized Moment Methods in Electromagnetics*, New York: John Wiley & Sons, 1990, ch. 6.

[13]   S. M. Rao, D. R. Wilton, and A. W. Glisson, "Electromagnetic scattering by surfaces of arbitrary shape," *IEEE Trans. Antennas and Propagation*, vol. AP-30, no. 3, pp. 409-418, May 1982.

[14]   Y. Ji, H. Wang, and T. H. Hubing, "A novel preconditioning technique and comparison of three formulations for the hybrid FEM/MoM method," *Appl. Computat. Electromagn. Soc. (ACES) J.*, vol. 15, pp. 103-114, July 2000.

[15]   J. J. Bowman, T. B. A. Senior, P. L. E. Uslenghi*, Electromagnetic and acoustic scattering by simple shapes*, Hemisphere Publishing Corporation, New York: 1987.

[16]   H. Wang, C. Guo, T. Hubing, J. Drewniak, T. Van Doren and R. DuBroff, "Application of higher-order FEM elements to the analysis of microstrip structures", *Proc. of the 2002 IEEE International Symposium on Electromagnetic Compatibility*, Minneapolis, MN, August 2002, pp. 1015-1019.

[17]   J. –M. Jin, *The Finite Element Method in Electromagnetic,* 2nd edition, New York: John Wiley & Sons, 2002.

[18]   D. M. Pozar, *Microwave Engineering*, 2nd edition, New York: John Wiley & Sons, 1998.

APPENDIX A

FEM analysis requires computation of two matrices. These two matrices are,

$$E_{ij} = \int_V \nabla \times \mathbf{w}_i \bullet \nabla \times \mathbf{w}_j \, dV \tag{A1}$$

$$F_{ij} = \int_V \mathbf{w}_i \bullet \mathbf{w}_j \, dV \cdot \tag{A2}$$

A. CT/LN TVFE

$$\mathbf{w}_i = l_i(L_{i1}\nabla L_{i2} - L_{i2}\nabla L_{i1}) \cdot \tag{A3}$$

B. Webb's unnormalized LT/QN TVFE
Edge element

$$\mathbf{w}_i^{e1} = l_i(L_{i1}\nabla L_{i2} - L_{i2}\nabla L_{i1}) \tag{A4}$$

$$\mathbf{w}_i^{e2} = l_i(L_{i1}\nabla L_{i2} + L_{i2}\nabla L_{i1}) \quad i = 1, \cdots 6 \tag{A5}$$

Face element

$$\mathbf{w}_i^{f1} = L_{i1}L_{i2}\nabla L_{i3} - L_{i1}L_{i3}\nabla L_{i2} \tag{A6}$$

$$\mathbf{w}_i^{f2} = L_{i1}L_{i2}\nabla L_{i3} - L_{i2}L_{i3}\nabla L_{i1} \quad i = 1, \cdots 4 \tag{A7}$$

B. Webb's normalized LT/QN TVFE
Edge element

$$\mathbf{w}_i^{e1} = L_{i1}\nabla L_{i2} - L_{i2}\nabla L_{i1} \tag{A8}$$

$$\mathbf{w}_i^{e2} = L_{i1}\nabla L_{i2} + L_{i2}\nabla L_{i1} \quad i = 1, \cdots 6 \tag{A9}$$

Face element

$$\mathbf{w}_i^{f1} = L_{i1}L_{i2}\nabla L_{i3} - L_{i1}L_{i3}\nabla L_{i2} \tag{A10}$$

$$\mathbf{w}_i^{f2} = L_{i1}L_{i2}\nabla L_{i3} - L_{i2}L_{i3}\nabla L_{i1} \quad i = 1, \cdots 4 \tag{A11}$$

C. Andersen's unnormalized LT/QN TVFE
Edge element

$$\mathbf{w}_i^{e1} = l_i(L_{i1}\nabla L_{i2} - L_{i2}\nabla L_{i1}) \tag{A12}$$

$$\mathbf{w}_i^{e2} = l_i(L_{i1} - L_{i2})(L_{i1}\nabla L_{i2} - L_{i2}\nabla L_{i1}) \quad i = 1, \cdots 6 \tag{A13}$$

Face element

$$\mathbf{w}_i^{f1} = L_{i1}L_{i2}\nabla L_{i3} - L_{i1}L_{i3}\nabla L_{i2} \tag{A14}$$

$$\mathbf{w}_i^{f2} = L_{i1}L_{i2}\nabla L_{i3} - L_{i2}L_{i3}\nabla L_{i1} \quad i = 1, \cdots 4 \tag{A15}$$

D. Andersen's normalized LT/QN TVFE
Edge element

$$\mathbf{w}_i^{e1} = L_{i1}\nabla L_{i2} - L_{i2}\nabla L_{i1} \tag{A16}$$

$$\mathbf{w}_i^{e2} = (L_{i1} - L_{i2})(L_{i1}\nabla L_{i2} - L_{i2}\nabla L_{i1}) \quad i = 1, \cdots 6 \tag{A17}$$

Face element

$$\mathbf{w}_i^{f1} = L_{i1}L_{i2}\nabla L_{i3} - L_{i1}L_{i3}\nabla L_{i2} \tag{A18}$$

$$\mathbf{w}_i^{f2} = L_{i1}L_{i2}\nabla L_{i3} - L_{i2}L_{i3}\nabla L_{i1} \quad i = 1, \cdots 4 \tag{A19}$$

Hao Wang received his B.S. degree in electrical engineering from Tsinghua University, Beijing, China in 1996, and M.S. and Ph.D. degrees in electrical engineering from the University of Missouri-Rolla, in 2000 and 2002, respectively.

From 1999 to 2002, he was with the Electromagnetic Compatibility Laboratory, University of Missouri-Rolla. He then joined the Advanced Systems Research Laboratory of Micron Technology, Boise, ID, as a signal integrity engineer. His research interests include numerical and experimental analysis of signal integrity and electromagnetic compatibility issues related to memory products, development of PCB design as needed to define next-generation DRAMs.
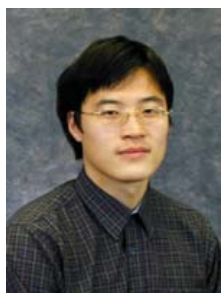
Chunlei Guo was born in China in 1975. He received the B.S. and M.S. degrees in electrical engineering from Tsinghua University, Beijing, China, in 1998 and 2000 respectively.

From 2000, he was with the Electromagnetic Compatibility Laboratory, University of Missouri-Rolla. His research interests include numerical and experimental analysis of signal integrity and electromagnetic compatibility issues related with high-speed digital systems.

Todd Hubing received the BSEE degree from the Massachusetts Institute of Technology, Cambridge, MA in 1980, the MSEE degree from Purdue University, West Lafayette, IN, in 1982, and the Ph.D. degree in electrical engineering from North Carolina State University, Raleigh, NC in 1988.

He is currently a Professor of electrical engineering at the University of Missouri-Rolla (UMR). Prior to joining UMR in 1989, he was an Electromagnetic Compatibility Engineer with IBM, Research Triangle Park, NC. Since joining UMR, the focus of his research has been measuring and modeling sources of electromagnetic interference. He is currently the 2002-2003 President of the IEEE Electromagnetic Compatibility Society.